Research Square

Preprints are preliminary reports that have not undergone peer review.
They should not be considered conclusive, used to inform clinical practice,
or referenced by the media as validated information.

# Compound heterozygous TDRD9 variants are associated with postmeiotic spermatid arrest and impaired LINE-1 suppression in a man with non-obstructive azoospermia

**HUIMEI ZHENG**

21107044@zju.edu.cn

Zhejiang University

**Yunbo Wang**

Zhejiang University

**Cheng Wu**

Zhejiang University

**Jianhua Chen**

Zhejiang University

**Xiaohang Yang**

Zhejiang University

**Yongmei Xi**

Zhejiang University

**Jingping Li**

Zhejiang University

**Research Article**

**Keywords:** male infertility, non-obstructive azoospermia, TDRD9, spermiogenesis, piRNA pathway, LINE-1

**Posted Date:** November 16th, 2026

**DOI:** https://doi.org/10.21203/rs.3.rs-10607537/v1

**License:** This work is licensed under a Creative Commons Attribution 4.0 International License.
Read Full License

**Additional Declarations:** No competing interests reported.

# *Compound heterozygous TDRD9 variants are associated with postmeiotic spermatid arrest and impaired LINE-1 suppression in a man with non-obstructive azoospermia*

Huimei Zheng[1,*], Yunbo Wang[3,4], Cheng Wu[1], Jianhua Chen[2], Xiaohang Yang[1,3,4], Yongmei Xi[1,3,4], Jingping Li [2,*]

[1]Zhejiang Key Laboratory of Precision Diagnosis and Therapy for Major Gynecological Diseases and [2]Department of Reproductive Endocrinology, the Women's Hospital, Zhejiang University School of Medicine, Hangzhou, Zhejiang, China;

[3]Center for Genetic Medicine, the Fourth Affiliated Hospital, Zhejiang University School of Medicine, Hangzhou, Zhejiang 310058, China;

[4]Institute of Genetics, Zhejiang Provincial Key Laboratory of Genetic & Developmental Disorders, Zhejiang University School of Medicine, Hangzhou, Zhejiang 310058, China.

*address correspondence to lijingpingself@zju.edu.cn; 21107044@zju.edu.cn

## Abstract

**Background:** Biallelic variants in *TDRD9,* a component of the germline piRNA pathway, have been associated with male infertility, but the stage-specific consequences of partial *TDRD9* dysfunction in humans remain unclear.

**Methods**: We studied a 22-year-old man with idiopathic non-obstructive azoospermia and his unaffected parents. Exome sequencing and segregation analysis were integrated with minigene splicing and protein-stability assays, testicular histology, acrosomal staining, meiotic chromosome spreads, exploratory bulk RNA sequencing, transposable-element profiling, and LINE-1 open reading frame 1 protein immunofluorescence. Obstructive azoospermia samples with preserved spermatogenesis served as controls where indicated.

**Results:** The proband carried a paternal splice-acceptor variant, c.1714-1G>C, and a maternal missense variant, c.2402A>C (p.Gln801Pro), in *TDRD9*. The splice variant caused exon 16 skipping and was predicted to generate p.Val572ArgfsTer5; p.Gln801Pro accelerated protein decay and was associated with reduced testicular TDRD9 abundance. Histology and acrosomal staining showed round-spermatid arrest, abnormal acrosome formation, and rare late spermatids. In the spermatocytes examined, chromosome-axis formation, synapsis, and sex-body formation showed no overt abnormalities. Exploratory transcriptomic findings were concordant with depletion of late spermiogenic programs. Evolutionarily young LINE-1 features were enriched among upregulated transposable-element features, and LINE-1 open reading frame 1 protein accumulated in spermatids.

**Conclusions:** This deeply phenotyped case supports an association between compound heterozygous *TDRD9* variants, postmeiotic spermatogenic failure, and impaired LINE-1 suppression. The data are compatible with residual TDRD9 activity permitting meiotic progression in the cells examined, but larger genotype-phenotype cohorts and direct piRNA analyses are required to test this model and assess clinical utility.

**Keywords:** male infertility; non-obstructive azoospermia; *TDRD9*; spermiogenesis; piRNA pathway; LINE-1

## Introduction

Male infertility affects approximately 7% of men and contributes to nearly half of infertility cases worldwide. Non-obstructive azoospermia (NOA) represents one of its most severe forms and is characterized by absent spermatozoa in the ejaculate due to intrinsic failure of spermatogenesis [1]. Although chromosomal abnormalities and Y-chromosome azoospermia factor microdeletions are established genetic causes, many men with idiopathic NOA remain without a molecular diagnosis [2]. Defining monogenic causes of NOA is clinically relevant because genetic findings may inform reproductive counseling, interpretation of infertility gene panels, and expectations for sperm retrieval in selected settings.

Spermatogenesis requires coordinated progression through mitotic expansion, meiotic chromosome pairing and recombination, and postmeiotic remodeling of haploid spermatids [3]. During this process, male germ cells must maintain genome integrity by suppressing transposable elements (TEs), particularly long interspersed nuclear element-1 (LINE-1) retrotransposons [4]. The PIWI-interacting RNA (piRNA) pathway is a germline defense system that guides PIWI-associated silencing of transposable elements at transcriptional and post-transcriptional levels. Disruption of piRNA pathway components in animal models causes LINE-1 derepression, meiotic defects, and male sterility [5, 6]. However, the stage-specific consequences of partial piRNA pathway impairment in human spermatogenesis remain incompletely defined.

Tudor domain-containing proteins (TDRDs) are key organizers of piRNA pathway complexes and germ cell development [7]. Among them, *TDRD9* encodes a

DExH-box RNA helicase–containing Tudor protein that interacts with the nuclear PIWI protein MIWI2 and contributes to LINE-1-targeted piRNA silencing [8]. In mice, *Tdrd9* deficiency leads to LINE-1 derepression, abnormal epigenetic regulation in male germ cells, meiotic failure, and complete male sterility. Human data are more limited [8, 9]. In contrast, human genotype-phenotype data remain limited. Recessive and compound heterozygous *TDRD9* variants have been reported in men with NOA, oligozoospermia, incomplete spermatogenic arrest, and partial meiotic abnormalities [10-13], suggesting a spectrum of *TDRD9*-associated spermatogenic failure. Nevertheless, whether hypomorphic *TDRD9* genotypes in humans primarily disrupt meiosis, postmeiotic spermiogenesis, or both remains unresolved.

Here, we investigated a man with idiopathic NOA carrying compound heterozygous *TDRD9* variants. We integrated exome sequencing and segregation analysis with minigene splicing assays, protein stability assays, testicular histology, meiotic chromosome spread analysis, and bulk testicular transcriptome/transposable-element profiling. The objective was to define the functional consequences of these *TDRD9* variants and to evaluate the relationship among residual TDRD9 activity, meiotic progression, postmeiotic spermiogenesis, and LINE-1 suppression in the human male germline.

## Materials and Methods

### Study participants and ethical approval

This single-patient translational study included a man with idiopathic NOA, his

available family members, and unrelated men with obstructive azoospermia (OA) and preserved spermatogenesis who provided control testicular tissue for the indicated assays. Participants were recruited at the Reproductive Medicine Center, Women's Hospital, Zhejiang University School of Medicine. Azoospermia was confirmed by two semen analyses. Karyotyping and Y-chromosome AZF microdeletion testing were negative. The proband underwent microdissection testicular sperm extraction; controls underwent clinically indicated biopsy. The study was approved by the Ethics Committee of Women's Hospital, Zhejiang University School of Medicine (IRB-20240397-R), and written informed consent was obtained from all participants.

**Whole-exome sequencing and Sanger validation**

Genomic DNA was isolated from peripheral blood using the HiPure Blood & Tissue DNA Kit (Magen). Whole-exome sequencing (WES) was performed on the Agilent SureSelect Human All Exon V6 + COSMIC system followed by paired-end sequencing on an Illumina platform. Reads were trimmed via Trimmomatic, quality-checked with FastQC, and aligned to the hg19 reference genome using BWA-MEM. Variant calling and annotation were completed using the Genome Analysis Toolkit (GATK) and ANNOVAR, respectively. Candidate variants were filtered under a rare recessive inheritance model using a minor allele frequency threshold of <0.001 across population databases (1000 Genomes, ESP6500, ExAC, gnomAD). Loss-of-function variants and missense mutations predicted deleterious by multiple *in silico* tools were prioritized based on testicular expression profiles. *TDRD9* variants (NM_153046.3) were validated by Sanger sequencing in the

pedigree using the following primers:

F1: 5’- ACTGTGGTGATGAGGAAATACA-3’,

R1: 5’- GCTTCTGACCATAAGATAAACCAAAGC -3’.

F2: 5’- GTCCTTTAGTGTTACCTCCC -3’,

R2: 5’- TCATCTTCTCTCTGCCCACT -3’.

**Testicular histology, immunofluorescence, and image analysis**

Testicular tissues were fixed in Bouin solution (>24 hours), paraffin-embedded, and sectioned at 5 μm for hematoxylin and eosin (H&E) staining. For immunofluorescence staining, paraffin-embedded sections were deparaffinized, subjected to antigen retrieval in citrate buffer, blocked with BSA, and incubated with primary antibodies overnight at 4°C. Sections were then incubated with fluorophore-conjugated secondary antibodies and counterstained with DAPI. TUNEL staining was performed using the TUNEL BrightGreen Apoptosis Detection Kit. Acrosome formation was assessed using Alexa Fluor 488-conjugated PNA lectin.

Primary antibodies used were: mouse anti-SYCP3 (Proteintech, 3-1-AP, 1:500), mouse anti-γH2AX (Cell Signaling, 80312, 1:1000), rabbit anti-DMC1 (Proteintech, 13714-1-AP, 1:500), and rabbit anti-L1-ORF1p (Abcam, ab245249, 1:100). Images were acquired using an Olympus FV1000 confocal microscope. Identical acquisition settings were used for comparisons within each staining experiment when quantification was performed.

## Structural modeling and conservation analysis

The structural effect of the p.Gln801Pro variant was assessed using DMFold and visualized with by Mol* 3D Viewer in PDB database. Evolutionary conservation of TDRD9 was evaluated by multiple sequence alignment of vertebrate orthologs using Clustal Omega. The analyzed sequences included human, mouse, rat, chicken, and zebrafish TDRD9 orthologs. Conservation plots were generated with SnapGene Viewer.

## Minigene splicing assay

To evaluate the effect of the c.1714-1G>C splice-site variant, a genomic fragment containing *TDRD9* Exon 15 (135 bp) -Intron 15 (983 bp)-Exon 16 (167 bp)-Intron 16 (91 bp)- Exon 17 (64 bp) was amplified and cloned into the pcDNA3.1 vector. Wild-type and mutant minigene constructs were transfected into HEK293T cells. After 48 hours, total RNA was extracted using TRIzol, reverse-transcribed, and amplified by polymerase chain reaction. Reverse-transcription polymerase chain reaction products were analyzed by agarose gel electrophoresis and confirmed by Sanger sequencing.

## Cell culture, transfection, cycloheximide chase, and Western blotting

HEK293T cells were cultured in DMEM (GIBCO) containing 10% FBS and 1% penicillin-streptomycin at 37°C under 5% $CO_2$. Cells were transfected with wild-type or p.Gln801Pro *TDRD9* plasmids using Lipo6000. For stability assays, cells were treated with 40 μg/mL cycloheximide (CHX, Merck, C7698-1G) and harvested at

designated time points. Lysates from cells or testicular tissue were prepared in RIPA buffer with protease and phosphatase inhibitors. Equal protein masses were separated via SDS-PAGE, transferred to PVDF membranes, and blotted with anti-TDRD9 (1:1000, Novus Biologicals, NB2-84297) and anti-β-tubulin antibodies. Protein bands were visualized using enhanced chemiluminescence and quantified via ImageJ. TDRD9 signals were normalized to β -tubulin and standardized to the 0-hour baseline across three independent cell-culture experiments.

**Meiotic chromosome spreads**

Fresh testicular tissue was minced, filtered, subjected to hypotonic treatment, and spread onto coverslips. Preparations were stained with anti-SYCP3 and anti-γH2AX. Spermatocytes were classified as leptotene, zygotene, pachytene, or diplotene based on axis morphology and γH2AX pattern. Because meiotic chromosome spreads were available from one proband and one control, cell counts were used to document the number and types of analyzable spermatocytes rather than for inferential statistical comparison.

**Transcriptomic and Transposable-Element Profiling**

Total RNA was extracted from isolated seminiferous tubules using TRIzol. Library construction utilized poly(A) mRNA enrichment with oligo-dT magnetic beads, followed by fragmentation, cDNA synthesis, adapter ligation, and amplification. Cleaned libraries were sequenced on an Illumina NovaSeq 6000 platform located at Wuhan Benagen Tech Solution Co. Ltd. (Wuhan, China; http://www.benagen.com).

Raw reads were aligned to the GRCh38 human reference genome using STAR (v2.7.11a) incorporating GENCODE v44 and RepeatMasker annotations. Gene-level abundances were summarized with GENCODE, while transposable-element (TE) and LINE-1 family expression features were quantified using TEtranscripts (v2.2.1) to accommodate multi-mapping reads. Differential expression analysis for both genes and TE features was executed using DESeq2. Candidate features were selected using a threshold of false discovery rate (FDR) <0.05 and an absolute log2 fold change >1. Given the N=1 nature of the patient source, these transcriptomic datasets were evaluated strictly as exploratory molecular correlates of the histopathological phenotype. LINE-1 features were stratified by evolutionary age, merging "Young active L1" and "Young L1" into a unified young LINE-1 category for down-stream enrichment testing. Gene set enrichment analysis (GSEA) was performed on the Reactome meiosis pathway to statistically evaluate meiotic transcripts.

**Statistical analysis**

*In vitro* protein-decay data are presented as mean ± SD from independent cell-culture experiments; wild-type and mutant constructs were compared using a two-tailed t test at the prespecified time point shown in the figure. Fisher's exact test was used to compare the proportion of young LINE-1 features among upregulated and downregulated LINE features. A two-sided $P < 0.05$ was considered statistically significant. Cell-level measurements and multiple tissue aliquots from one person were not treated as independent biological replicates. Meiotic-stage distributions and

immunofluorescence measurements from the single proband were therefore interpreted descriptively.

## Results

### Clinical phenotype and identification of compound heterozygous *TDRD9* variants

The proband was a 22-year-old man evaluated for primary infertility. Azoospermia was confirmed on two independent semen analyses. Serum follicle-stimulating hormone, luteinizing hormone, testosterone, estradiol, and prolactin concentrations were within institutional reference ranges (Supplemental Table 1). Cytogenetic testing showed a 46, XY karyotype, and Y-chromosome azoospermia factor microdeletion testing was negative.

Histological examination of testicular biopsy sections showed seminiferous tubules containing spermatogonia, spermatocytes, and round spermatids, with near absence of elongated spermatids, consistent with postmeiotic maturation arrest rather than Sertoli-cell-only syndrome or complete meiotic arrest (Fig. 1A and B). TUNEL staining showed an increased number of apoptotic germ cells in the proband compared with OA controls with preserved spermatogenesis (Fig. 1C and D).

Whole-exome sequencing (WES) modeled under a rare recessive inheritance pattern identified a novel compound heterozygous mutation in *TDRD9* (NM_153046.3): a paternal canonical splice-acceptor variant, c.1714-1G>C, and a

maternal missense variant, c.2402A>C, p.Gln801Pro. Sanger sequencing confirmed that the two variants were present *in trans* in the proband and heterozygous in the unaffected parents (Fig. 1E and F). Both variants were absent or extremely rare in population databases queried at the time of analysis, and the p.Gln801 residue was conserved across vertebrate orthologs (Fig. 1G). These findings prioritized biallelic *TDRD9* variation as the primary candidate genetic diagnosis.

## The c.1714-1G>C and p.Gln801Pro variants impair *TDRD9* splicing and protein stability

Because c.1714-1G>C disrupts the canonical splice acceptor site upstream of exon 16, we tested its effect using a minigene splicing assay. The mutant construct generated a smaller reverse-transcription polymerase chain reaction product than the wild-type construct (Fig. 2A). Sanger sequencing of the product confirmed skipping of exon 16, which is predicted to introduce a frameshift and premature stop codon, p.Val572ArgfsTer5 (Fig. 2B and C).

We next evaluated the p.Gln801Pro missense variant. Structural modeling predicted that substitution of glutamine by proline at residue 801 would perturb the local protein environment (Supplemental Fig.1). In testicular sections, TDRD9 immunofluorescence was reduced in the proband compared with OA controls (Fig. 2D). Western blotting of testicular lysates also showed lower TDRD9 protein abundance in the proband sample (Fig. 2E).

To determine whether p.Gln801Pro affects protein turnover, wild-type and mutant *TDRD9* constructs were expressed in HEK293T cells and treated with cycloheximide

(CHX). The mutant TDRD9 (p.Gln801Pro) protein showed accelerated decay compared with wild-type TDRD9 over the 8-hour chase period (Fig. 2F and G). At 8 hours, relative mutant TDRD9 abundance was 28% of baseline compared with 94% for wild-type TDRD9. These data indicate that the two alleles affect TDRD9 through distinct mechanisms: catastrophic exon skipping on the paternal allele and severe protein destabilization on the maternal allele.

**Cytological analyses support postmeiotic spermatid arrest without overt meiotic chromosome abnormalities**

Histological examination of the proband testis showed seminiferous tubules containing spermatogonia, spermatocytes, and round spermatid-like cells, whereas late spermatids were rarely observed in the examined biopsy sections. To further assess postmeiotic spermatid differentiation, we performed PNA lectin staining, which labels the developing acrosome. In OA controls with preserved spermatogenesis, PNA localized asymmetrically as a cap-like signal over round spermatid nuclei. In the proband, PNA-positive round spermatids were present, but the signal frequently appeared perinuclear, circumferential, or poorly polarized rather than cap-like, consistent with abnormal acrosome formation during early spermiogenesis (Fig. 3A and B).

Because *TDRD9* deficiency in model systems has been associated with meiotic failure, we next examined meiotic progression in the proband. DMC1 staining in testicular sections did not show an obvious loss or abnormal distribution of recombination-associated spermatocytes compared with controls (Fig. 3A and B).

Meiotic chromosome spreads from the proband contained leptotene, zygotene, pachytene, and diplotene spermatocytes. Co-staining for SYCP3 and γH2AX showed formation of synaptonemal complex axes, sex chromosome body formation at the pachytene stage, and no overt defect in chromosome synapsis in the cells examined (Fig. 3C and D). Descriptive scoring of these analyzable nuclei confirmed a normal distribution across meiotic stages (Fig. 3E).

Consistent with these cytological observations, an exploratory transcriptome-based assessment, gene set enrichment analysis of the global transcriptomic data using the curated Reactome meiosis gene set showed no significant coordinated dysregulation or enrichment suppression in the proband testis (adjusted P = 0.992; nominal P = 0.837; Fig. 3F). Taken together, these cytological and transcriptomic evaluations demonstrate that meiotic chromosome pairing, synapsis, and recombination remain entirely intact under this genotype, isolating the pathological arrest exclusively to the post-meiotic phase.

**Exploratory testicular transcriptomics supports late spermatid depletion**

To characterize the molecular underpinnings of this phenotype, we performed exploratory bulk RNA sequencing using three seminiferous-tubule aliquots from the proband and samples from three independent OA controls. The three proband aliquots were technical or intra-individual samples rather than independent biological replicates. Principal component analysis separated the proband-derived libraries from OA control libraries and showed within-individual clustering of the proband aliquots (Supplementary Fig. 2). This pattern documents technical consistency but does not

provide population-level replication.

Using an exploratory DESeq2 comparison, 5,015 genes met the exploratory differential-expression thresholds, including 1,213 upregulated and 3,802 downregulated genes in the proband-derived libraries (FDR <0.05, absolute log2 fold change >1; Supplemental Fig. 3A; Supplemental Table 2). Downregulated genes were enriched for spermatid development, sperm motility, sperm-egg recognition, acrosomal vesicle, sperm head, and sperm flagellum terms (Supplemental Fig. 3B). Upregulated genes were enriched for extracellular matrix organization, cell adhesion, angiogenesis, and innate immune response terms (Supplemental Fig. 3C). TDRD9 expression was reduced, whereas other Tudor domain-containing genes showed no coordinated compensatory change (Supplemental Fig. 4). Overall, the bulk transcriptome profile is largely concordant with the histologically observed late spermatid depletion and postmeiotic spermiogenic arrest.

**Young LINE-1 expression and ORF1p accumulation indicate impaired LINE-1 silencing**

Given the established role of TDRD9 in transposable-element silencing [8, 9], we quantified transposable-element (TE) expression from the bulk RNA-sequencing data. TEs are genetic elements capable of moving within the genome via a copy-and-paste mechanism (class I retrotransposons) or a cut-and-paste mechanism (class II DNA transposons). Class I TEs are mainly subdivided into long interspersed nuclear elements (LINEs), short interspersed nuclear elements (SINEs), and long terminal repeat (LTR ) groups [14]. Exploratory differential expression analysis identified 793

upregulated and 4,612 downregulated TE features in the proband testis (adjusted P <0.05; absolute log2 fold change >1; Fig. 4A). LINE elements represented the largest class among upregulated transposable elements, with 235 upregulated LINE features (Fig. 4B).

To further characterize the derepression pattern of LINEs, we stratified these loci based on their evolutionary ages and retrotransposition potential. These categories ranged from Young Active L1 (e.g., L1HS), which retain intact open reading frames and full transposition capacity, to Intermediate (Mid) and ancient (Old) L1 elements that are largely degraded and transpositionally inert [15, 16]. Young active and young LINE-1 features were overrepresented among upregulated LINE features compared with downregulated LINE features (23/235=9.8% vs. 80/1904=4.2%; odds ratio, 2.47; 95% CI, 1.52-4.02; two-sided Fisher exact $P < 0.001$; Fig. 4C). In contrast, mid-age and old LINE classes accounted for most downregulated LINE features, a pattern consistent with global changes in germ-cell composition.

We next assessed LINE-1 protein expression by immunofluorescence for LINE-1 open reading frame 1 protein (ORF1p) [17]. ORF1p signal was low or undetectable in OA control testes but was increased in spermatids from the proband (Fig. 4D). Descriptively, 61% of scored spermatids were ORF1p-positive in the proband compared with 12% in the control samples, and mean fluorescence intensity was 5.02-fold higher. Because these cell-level observations were derived from one affected individual, no population-level inference was made. Together with the transposable-element profile, these findings are consistent with impaired LINE-1

suppression in the *TDRD9*-variant testis.

## Discussion

In this study, we identified compound heterozygous *TDRD9* variants in a man with idiopathic NOA and performed genetic, cellular, transcriptomic, and functional analyses to define the associated spermatogenic defect. One allele, c.1714-1G>C, disrupted normal splicing and caused exon 16 skipping, whereas the missense allele, c.2402A>C, p.Gln801Pro, accelerated TDRD9 protein decay. Testicular histology and acrosomal staining localized the developmental arrest predominantly to the postmeiotic spermatid stage, with abnormal acrosome formation and near absence of late spermatids. In contrast, meiotic chromosome spread analysis did not reveal overt abnormalities in synapsis, recombination-associated markers, or sex body formation in the cells examined. Together with increased expression of young LINE-1 elements and accumulation of LINE-1 ORF1p in spermatids, these findings support a model in which residual TDRD9 activity suffices for meiotic progression but falls short of supporting postmeiotic spermiogenesis and LINE-1 suppression in the human male germline.

Human *TDRD9*-associated infertility spans a range of spermatogenic phenotypes. Since the first report of a homozygous frameshift *TDRD9* variant in men with NOA, additional biallelic or potentially damaging *TDRD9* variants have been described in men with oligozoospermia, incomplete spermatogenic arrest, and NOA with partial

meiotic abnormalities [10-12, 18]. The available cases remain few and differ in the depth of phenotyping, but they suggest a possible genotype–phenotype relationship. Severe truncating alleles that are predicted to abolish major functional domains have been associated with maturation arrest or mixed defects, whereas a previously reported compound heterozygous genotype retaining partial normal transcript was associated with oligozoospermia [10-12]. In the present case, the splice-site allele is predicted to be loss-of-function, whereas the p.Gln801Pro allele produces an unstable but detectable protein. This allelic combination is consistent with a hypomorphic *TDRD9* genotype rather than complete loss of function. The observation that meiosis was not overtly disrupted in this patient, despite marked impairment of spermatid differentiation, supports the possibility that different stages of human spermatogenesis have different thresholds for TDRD9 activity (Table 1).

This stage-specific interpretation also helps reconcile the current human findings with data from model systems. In mice, *Tdrd9* deficiency causes LINE-1 derepression, abnormal germline epigenetic regulation, meiotic failure, and male sterility [8, 9]. The more severe meiotic phenotype in complete knockout models may reflect the absence of residual TDRD9 function, species-specific requirements for TDRD9 during male germ-cell development, or both. A useful comparison can also be made with *TDRD12*, another piRNA pathway component. Pathogenic *TDRD12* variants in humans and knockout models have been linked to meiotic arrest accompanied by LINE-1 ORF1p accumulation in spermatocytes [19]. By contrast, in the present *TDRD9* case, ORF1p accumulation was most evident in spermatids, and cytological analysis did not

identify a major meiotic chromosome defect. These differences suggest that piRNA pathway disruption does not necessarily produce a uniform meiotic-arrest phenotype in humans; instead, the affected developmental stage may depend on the specific component, mutation type, and residual pathway activity.

The LINE-1 findings provide a mechanistic link between the *TDRD9* genotype and postmeiotic germ-cell failure, though they must be interpreted cautiously. Transposable-element analysis showed that upregulated LINE elements were enriched for evolutionarily young LINE-1 classes, whereas many downregulated transposable elements were older or likely reflected the global loss of late germ-cell populations. This pattern is biologically plausible because only a small subset of human LINE-1 copies remain young, full-length, and potentially active [20, 21]. The increase in LINE-1 ORF1p protein in spermatids provides protein-level support for impaired LINE-1 silencing in the proband testis. However, because small RNA sequencing was not performed, we cannot directly determine whether piRNA abundance, piRNA sequence composition, 1U bias, 10A bias, or ping-pong signatures were altered. Therefore, the combined transcriptomic and ORF1p findings are best interpreted as evidence of impaired LINE-1 suppression consistent with compromised TDRD9-dependent piRNA pathway activity, rather than definitive proof of global piRNA pathway collapse.

The bulk testicular transcriptome further supported the cellular phenotype but was not used to infer direct transcriptional targets of *TDRD9*. The downregulated gene set was enriched for spermatid development, sperm motility, acrosomal vesicle, sperm

head, and sperm flagellum terms, consistent with the histological absence of late spermatids. Conversely, upregulated genes were enriched for extracellular matrix, cell adhesion, angiogenesis, and innate immune response pathways, likely reflecting changes in somatic-cell composition, stromal remodeling, or secondary tissue responses associated with germ-cell depletion. Because the proband RNA-sequencing libraries were derived from aliquots of a single affected individual, these transcriptomic data should be regarded as exploratory molecular correlates of the tissue phenotype. This conservative interpretation is important because bulk RNA sequencing of testicular tissue is strongly influenced by germ-cell composition, especially in samples with severe spermatogenic arrest.

Clinically, this case expands the phenotypic spectrum of *TDRD9*-associated male infertility and supports inclusion of *TDRD9* in the interpretation of genetic testing for idiopathic NOA, particularly in men with normal karyotype and negative Y-chromosome azoospermia factor testing. The findings also highlight the importance of variant-level functional assessment. A canonical splice-site variant and a destabilizing missense variant may have different biological consequences from complete truncating variants or splice variants that retain partial wild-type transcript. For reproductive counseling, identifying biallelic *TDRD9* variants may help explain the etiology of spermatogenic failure and may inform discussions about inheritance risk. However, the ability of *TDRD9* genotype to predict sperm retrieval outcome remains uncertain and will require larger genotype-phenotype datasets with standardized histology and microdissection testicular sperm extraction outcomes.

Several limitations should be acknowledged. This is a single-patient study, and additional individuals with comparable biallelic *TDRD9* genotypes are needed to validate the proposed stage-specific model. Patient material was limited, precluding small RNA sequencing, rescue experiments and knock-in modelling. The absence of overt meiotic defects should be interpreted in the context of the number and quality of analyzable spermatocytes rather than as proof that all aspects of meiosis were normal. Despite these limitations, the combination of segregation, splicing, protein-stability, testicular cytology and LINE-1 protein data supports a meiosis-sparing, postmeiotic arrest phenotype associated with hypomorphic *TDRD9* variation in human NOA.

## Conclusions

In this patient, compound heterozygous *TDRD9* variants impaired splicing and protein stability and were associated with round-spermatid arrest, abnormal acrosome formation, and increased LINE-1 expression. Meiotic cytology did not reveal overt abnormalities in the spermatocytes examined. These findings extend the human phenotypic spectrum of *TDRD9*-associated infertility and motivate larger cohorts and direct piRNA profiling to test whether residual TDRD9 activity produces stage-specific effects.

## List of abbreviations

AZF: azoospermia factor; CHX: cycloheximide; FDR: false discovery rate; GSEA: gene set enrichment analysis; LINE-1: long interspersed nuclear element-1; NOA: non-obstructive azoospermia; OA: obstructive azoospermia; ORF1p: open reading

frame 1 protein; piRNA: PIWI-interacting RNA; TE: transposable element; TDRD9: Tudor domain-containing protein 9; WES: whole-exome sequencing.

## Declarations

### Ethics approval and consent to participate

The study was approved by the Ethics Committee of Women's Hospital, Zhejiang University School of Medicine (approval no. IRB-20240397-R), and was conducted in accordance with the Declaration of Helsinki. Written informed consent was obtained from all participants

### Consent for publication

Not applicable.

### Availability of data and materials

The RNA-seq data generated during this study have been deposited in the Gene Expression Omnibus (GEO) under accession number GSE343307, and are publicly available at https://www.ncbi.nlm.nih.gov/geo/query/acc.cgi?acc=GSE343307. The whole-exome sequencing data are not publicly available due to patient privacy protection, but are available from the corresponding author upon reasonable request subject to institutional ethics approval. All other data generated or analyzed during this study are included in this published article and its supplementary information files.

## Competing interests

The authors declare that they have no competing interests.

## Funding

This study was supported by grants from the National Natural Science Foundation of China (82571846), Zhejiang Medical and Health Science and Technology Project (2025KY085) and Zhejiang Science and Technology Plan for Disease Prevention and Control (2026JKY150).

## Authors' contributions

HZ and JL conceived and designed the study, interpreted the data, and drafted the manuscript. HZ, YW, CW, and JC performed experiments and analysed data. XY and YX contributed reagents and critically reviewed the manuscript. All authors read and approved the final manuscript.

## Acknowledgements

The authors wish to thank all the patients and their family members for participating in this study. The authors thank Jingyao Chen from the Core Facilities, Zhejiang University School of Medicine, for technical support.

## Figure legends

Figure 1. Clinical phenotype and genetic analysis of the proband carrying compound heterozygous *TDRD9* variants. (A, B) Representative H&E-stained testicular sections from an OA control (A) and the proband (B). The proband exhibits a maturation arrest

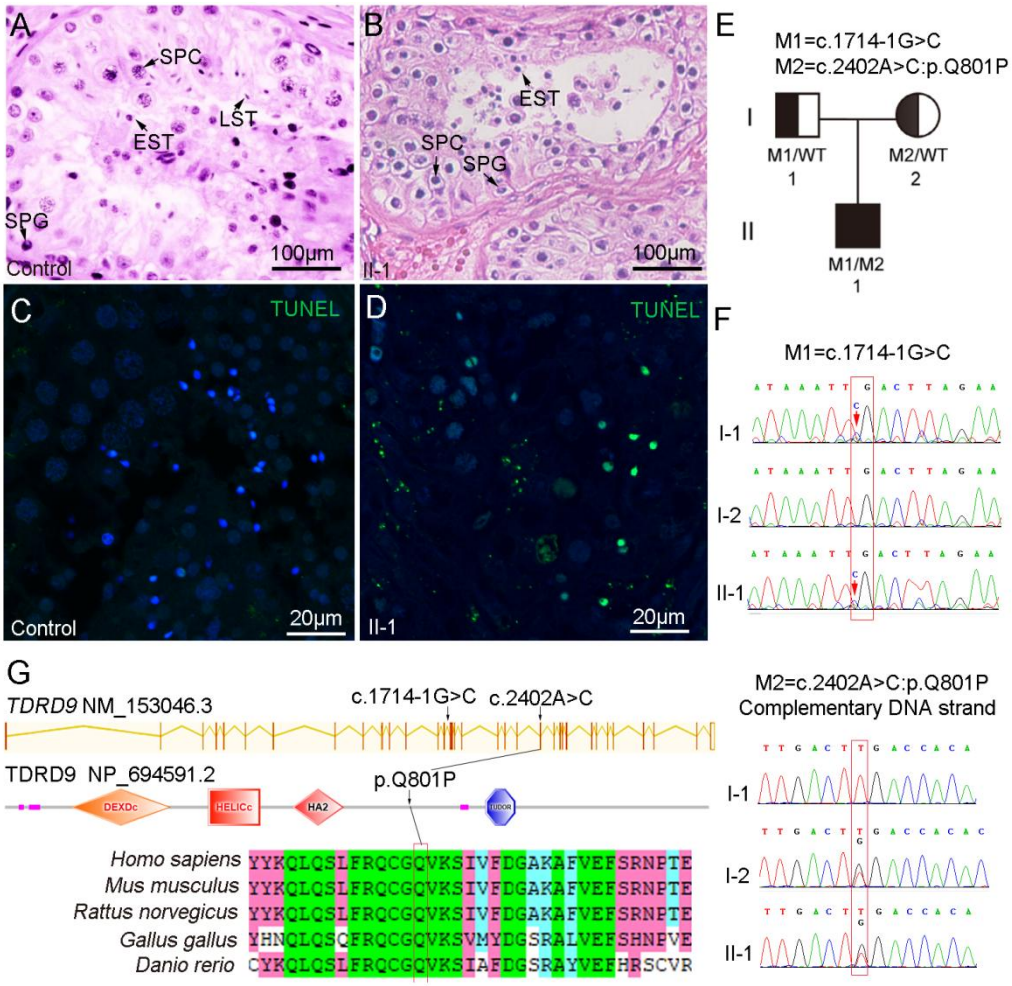
phenotype characterized by the absence of late spermatids. Abbreviations: SG, spermatogonia; SC, spermatocytes; EST, early spermatid; LST, late spermatid. Scale bar: 10 μm. (C, D) TUNEL assay (green) combined with DAPI nuclear staining (blue) on paraffin sections from an OA control (C) and the proband (D). (E) Pedigree of the family showing congenital azoospermia in the proband (individual II-1). (F) Sanger sequencing chromatograms confirming compound heterozygous *TDRD9* variants in the proband, the splicing variant c.1714-1G>C (paternal allele) and the missense variant c.2402A>C (p. p.Gln801Pro, maternal allele). (G) Schematic of *TDRD9* genomic structure and protein domains, showing the positions of the two variants. Conservation analysis of the p.Gln801 residue across vertebrate orthologs is shown below.

Figure 2. Functional characterization of the *TDRD9* variants. (A) Agarose gel electrophoresis of RT-PCR products from the minigene splicing assay. The c.1714-1G>C mutant construct generated a smaller amplicon than the wild-type construct. (B) Sanger sequencing of the RT-PCR product confirmed the skipping of exon 16 in the proband's *TDRD9* transcript. (C) Schematic model of the predicted effect of the c.1714-1G>C splice-site mutation on *TDRD9* mRNA processing. (D) Immunofluorescence staining for TDRD9 (green) in testicular sections from a control OA and the proband. Nuclei are counterstained with DAPI (blue). (E) Western blot analysis shows reduced TDRD9 protein levels in testis lysates from the proband compared to an OA control. (F, G) The p.Q801P missense variant reduces TDRD9 protein stability. (F) Representative western blot of HEK293T cells expressing wild-type (WT) or mutant (MUT, p.Q801P) TDRD9 following treatment with cycloheximide (CHX) for the indicated times. (G) Quantification of TDRD9 protein abundance during cycloheximide chase experiments. TDRD9 signal was normalized to β-tubulin and then to the 0-hour time point. Data are presented as mean ± SD from three independent experiments. **P < 0.01. a.u., arbitrary units; CHX, cycloheximide; WT, wild-type; MUT, mutant.

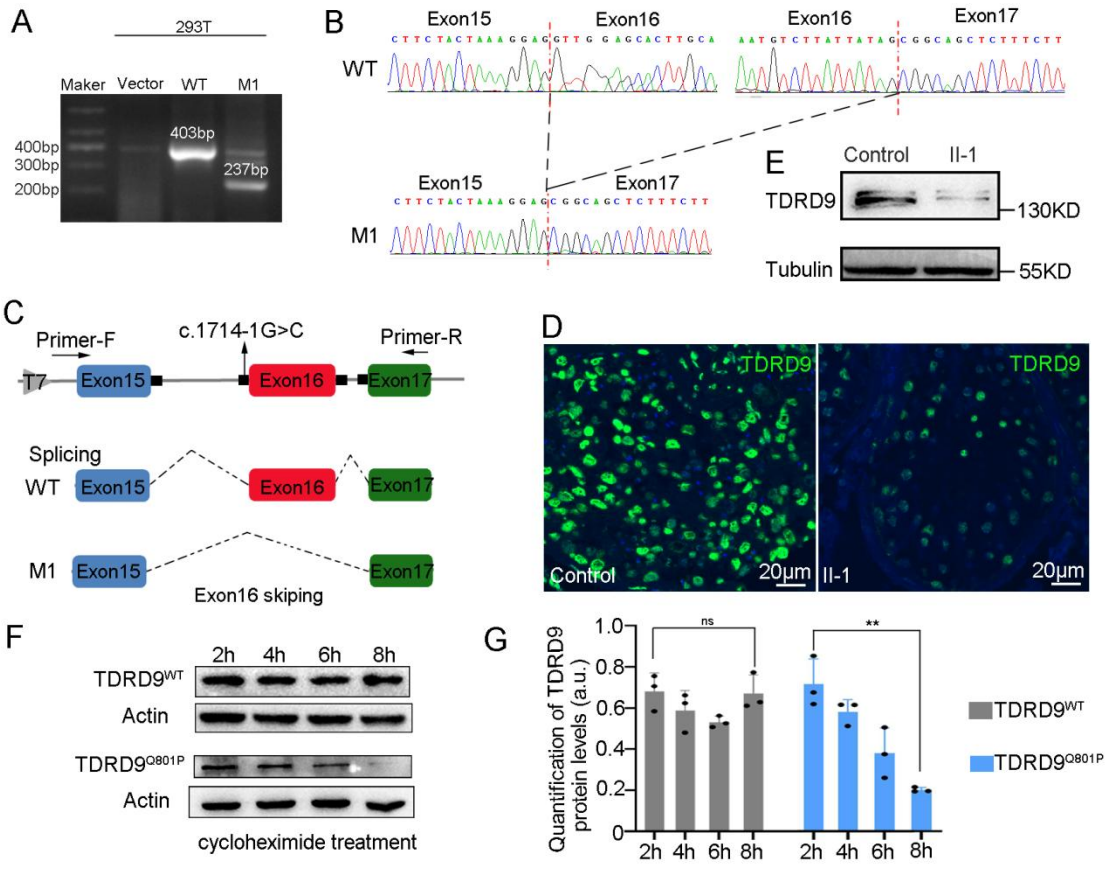
Figure 3. *TDRD9* compound heterozygous mutations disrupt late spermiogenesis without impairing meiosis. (A, B) Testicular sections from an OA control (A) and the proband (B) stained with PNA lectin (green) and the meiotic recombinase DMC1 (red). Nuclei are counterstained with DAPI (blue). In the control, PNA localized asymmetrically as a cap-like signal over round spermatid nuclei. In the proband, PNA-positive round spermatid-like cells were present, but the signal frequently appeared perinuclear, circumferential, or poorly polarized. DMC1-positive spermatocytes were detected in the proband without an obvious loss or abnormal distribution in the sections examined. (C, D) Representative meiotic chromosome spreads from spermatocytes co-stained for the synaptonemal complex protein SYCP3 (red) and the DNA damage/sex body marker γH2AX (green). (C) Control and (D) proband spreads show showed SYCP3-positive chromosome axes and γH2AX sex-body staining in pachytene cells. No overt defects in chromosome-axis formation, synapsis, or sex-body formation were detected in the cells examined. (E) Descriptive scoring of analyzable meiotic chromosome-spread nuclei from one OA control and the proband. Cells were classified as leptotene (L), zygotene (Z), pachytene (P), or diplotene (D) based on SYCP3-axis morphology and γH2AX staining pattern. Counts are descriptive only; no statistical comparison was performed because each group contained one individual. (F) Gene Set Enrichment Analysis (GSEA) plot of the Reactome Meiosis pathway, showing no significant enrichment in the *TDRD9*-mutant testis.

Figure 4. Transposable element (TE) derepression and LINE-1 activation in the *TDRD9*-mutant testis. (A) Volcano plot of differentially expressed TE features. Global view of TE expression changes in the *TDRD9*-mutant testis compared to the OA control. Upregulated features are shown in orange, downregulated features in blue, and non-significant features in gray. (B) Distribution of upregulated and downregulated TE feature by class. Bar plot showing the counts of significantly upregulated (orange) and downregulated (blue) TE feature for each major TE class: LTR (long terminal repeat), LINE (long interspersed nuclear element), SINE (short

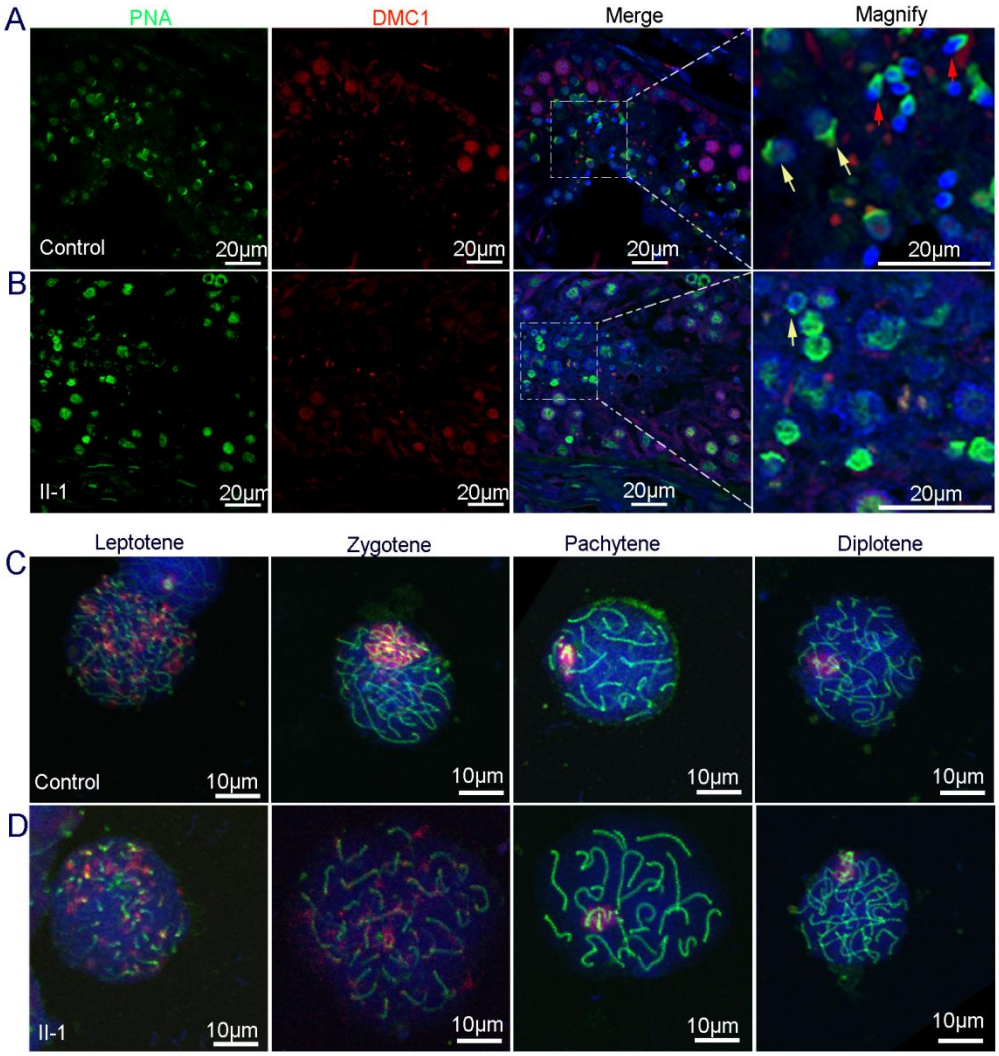
interspersed nuclear element), DNA (DNA transposon), and other (unclassified). (C) Distribution of dysregulated LINE elements by evolutionary age. Pie charts show the proportional distribution of each subgroup, with numerical values representing the actual counts of feature in each category. Young LINEs are overrepresented in the upregulated group despite their overall lower absolute number, consistent with selective reactivation of evolutionarily young retroelements. (D) Immunofluorescence detection of LINE-1 ORF1p in testicular sections. Representative images of testicular tissue from the OA control (upper panels) and the *TDRD9*-mutant proband (lower panels). L1-ORF1p (red) was detected using a specific antibody, and nuclei were counterstained with DAPI (blue). The proband's testis showed strong and specific ORF1p accumulation, predominantly localized within the cytoplasm of spermatids (arrows). Scale bar: 20 μm.


A
SPC
LST
EST
SPG
Control
100μm
B
EST
SPC
SPG
II-1
100μm
E
M1=c.1714-1G>C
M2=c.2402A>C:p.Q801P
I
M1/WT
1
M2/WT
2
II
M1/M2
1
C
TUNEL
Control
20μm
D
TUNEL
II-1
20μm
F
M1=c.1714-1G>C
I-1
I-2
II-1
G
TDRD9 NM_153046.3
c.1714-1G>C
c.2402A>C
TDRD9 NP_694591.2
p.Q801P
DEXDc
HELICc
HA2
TUDOR
Homo sapiens YYKQLQSLFRQCGQVKSIVFDGAKAFVEFSRNPTE
Mus musculus YYKQLQSLFRQCGQVKSIVFDGAKAFVEFSRNPTE
Rattus norvegicus YYKQLQSLFRQCGQVKSIVFDGAKAFVEFSRNPTE
Gallus gallus YHNQLQSQFRQCGQVKSVMYDGSRALVEFSHNPVE
Danio rerio CYKQLQSLFRQCGQVKSIAFDGSRAYVEFHRSCVR
M2=c.2402A>C:p.Q801P
Complementary DNA strand
I-1
I-2
II-1

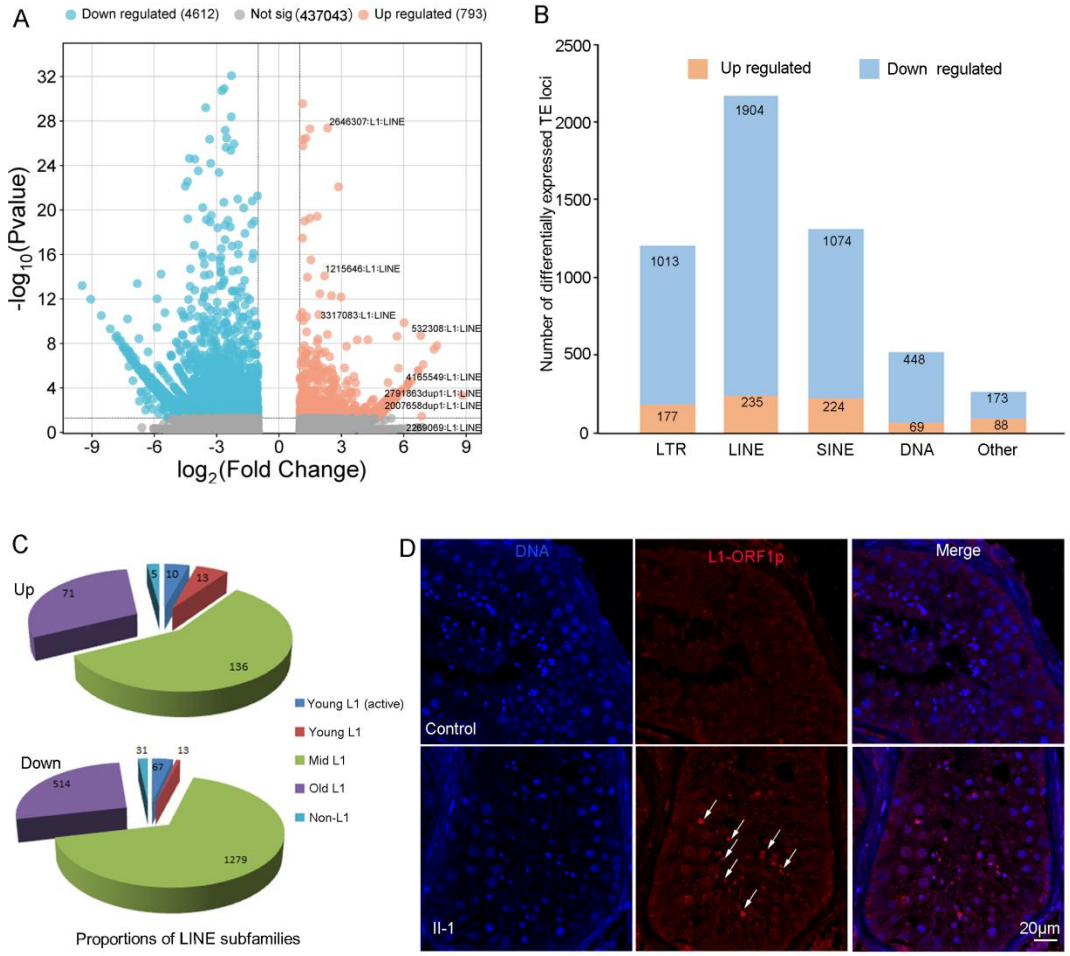
552


A
293T
Maker
Vector
WT
M1
400bp
300bp
200bp
403bp
237bp
B
Exon15
Exon16
Exon16
Exon17
WT
Exon15
Exon17
M1
E
Control
II-1
TDRD9
130KD
Tubulin
55KD
C
Primer-F
c.1714-1G>C
Primer-R
T7
Exon15
Exon16
Exon17
Splicing
WT
Exon15
Exon16
Exon17
M1
Exon15
Exon17
Exon16 skiping
D
TDRD9
TDRD9
Control
20μm
II-1
20μm
F
2h
4h
6h
8h
TDRD9WT
Actin
TDRD9Q801P
Actin
cycloheximide treatment
G
Quantification of TDRD9 protein levels (a.u.)
1.0
0.8
0.6
0.4
0.2
0
ns
**
2h
4h
6h
8h
2h
4h
6h
8h
TDRD9WT
TDRD9Q801P

553


A
PNA
DMC1
Merge
Magnify
Control
20μm
B
II-1
C
Leptotene
Zygotene
Pachytene
Diplotene
10μm
D
E
OA(n=185)
Proband (159)
Population(%)
23
29
38
39
107
80
17
15
L
Z
P
D
F
REACTOME_MEIOSIS
p.adjust=0.992
pvalue=0.837
Running Enrichment Score
Ranked List Metric
Rank in Ordered Dataset

554


A
Down regulated (4612)
Not sig (437043)
Up regulated (793)
-log10(Pvalue)
log2(Fold Change)
2646307:L1:LINE
1215646:L1:LINE
3317083:L1:LINE
532308:L1:LINE
4165549:L1:LINE
2791863dup1:L1:LINE
2007658dup1:L1:LINE
2269069:L1:LINE
B
Up regulated
Down regulated
Number of differentially expressed TE loci
1013
177
1904
235
1074
224
448
69
173
88
LTR
LINE
SINE
DNA
Other
C
Up
71
5
10
13
136
Down
514
31
67
13
1279
Young L1 (active)
Young L1
Mid L1
Old L1
Non-L1
Proportions of LINE subfamilies
D
DNA
L1-ORF1p
Merge
Control
II-1
20μm

555

556

**Table 1. Comparative analysis of reported *TDRD9* mutations and associated phenotypes**

| **Feature** | **Arafat *et al.* (2017)[10]** | **Tang *et al.* (2024)[11]** | **Zhou *et al.* (2024)[18]** | **Hu *et al.* (2025)[12]** | **Hu *et al.* (2025)[12]** | **Our study** |
|---|---|---|---|---|---|---|
| **Mutation type** | Homozygous (c.720_723 del TAGT) | Compound heterozygous (c.1115 + 3A > G) and (c.958delC) | Homozygous (c.2737T > C) | Homozygous (c.179_186del) | Homozygous (c.3587T>C) | Compound heterozygous (c.1714-1G>C) and (c.2402A>C) |
| **Predicted protein impact** | Truncated protein (p.S241Pfs*4) | p.Asn373X (partial WT transcript retention) and (p.H320Ifs*28) | Single amino acid substitution (p.F913L) | Truncated protein (p.Q61Gfs*22) | Single amino acid substitution (p.L1196P) | Truncated protein (p.V572Rfs*5) and Single amino acid substitution (p.Q801P) |
| **Protein detection** | Reduced level detected by IF (anti-N-terminus) | Not assessed | Not assessed | Reduced level detected by WB | Reduced level detected by WB | Reduced level (detected by WB and IF) + destabilized (CHX assay) |
| **Clinical phenotype** | NOA | Oligozoospermia | NOA | NOA | NOA | NOA |

| | | | | | | |
|---|---|---|---|---|---|---|
| **Histology** | Maturation arrest with focal SCOS (presence of SG, SC, reduced RS and ES) | Not assessed; Likely incomplete maturation arrest (oligozoospermia) | Not assessed | Maturation arrest (presence of SG, SC, RS and reduced ES) | Not assessed | Maturation arrest (presence of SG, SC, RS and reduced ES) |
| **Meiosis** | Partially affected (presence of spermatids) | Not assessed (sperm present) | Not assessed | Partial meiotic defects (Partial γH2AX abnormal) | Not assessed | Intact (SCP3/γH2AX/DMC1 normal) |
| **Spermiogenesis** | Arrested | Partially affected | Unknown | Arrested | Unknown | Arrested |
| **Key mechanistic insight** | First human *TDRD9* mutation | Partial WT transcript retention yields residual sperm | Domain-specific disruption | Position-dependent truncation may impact differently | Domain-specific disruption | Stability defect preserves meiosis but blocks spermiogenesis |

Abbreviations: NOA, non-obstructive azoospermia; IF, immunofluorescence; WB, western blot; WT, wild-type. SG, spermatogonia; SC, spermatocytes; RS, round spermatids; ES, elongated spermatids.

561

## References


[1] Wang X, Nie L, Hong Z, Li L, Fan Q, Ma B, et al. Genetic and epigenetic insights into non-obstructive azoospermia: mechanisms, biomarkers, and clinical perspectives. Reprod Biol Endocrinol. 2025;23:159.

[2] Krausz C, Riera-Escamilla A. Genetics of male infertility. Nature Reviews Urology. 2018;15:369-84.

[3] Nishimura H, L'Hernault SW. Spermatogenesis. Current Biology. 2017;27:R988-R94.

[4] De Fazio S, Bartonicek N, Di Giacomo M, Abreu-Goodger C, Sankar A, Funaya C, et al. The endonuclease activity of Mili fuels piRNA amplification that silences LINE1 elements. Nature. 2011;480:259-63.

[5] Gou L-T, Gao Y, Kang J-Y, Wang X, Chen H, Hua M-M, et al. Reply to Lack of evidence for a role of PIWIL1 variants in human male infertility. Cell. 2021;184:1943-4.

[6] Weick E-M, Miska EA. piRNAs: from biogenesis to function. Development. 2014;141:3458-71.

[7] Gan B, Chen S, Liu H, Min J, Liu K. Structure and function of eTudor domain containing TDRD proteins. Critical Reviews in Biochemistry and Molecular Biology. 2019;54:119-32.

[8] Shoji M, Tanaka T, Hosokawa M, Reuter M, Stark A, Kato Y, et al. The TDRD9-MIWI2 Complex Is Essential for piRNA-Mediated Retrotransposon Silencing in the Mouse Male Germline. Dev Cell. 2009;17:775-87.

[9] Wenda JM, Homolka D, Yang Z, Spinelli P, Sachidanandam R, Pandey RR, et al. Distinct Roles of RNA Helicases MVH and TDRD9 in PIWI Slicing-Triggered Mammalian piRNA Biogenesis and Function. Dev Cell. 2017;41:623-+.

[10] Arafat M, Har-Vardi I, Harlev A, Levitas E, Zeadna A, Abofoul-Azab M, et al. Mutation in TDRD9 causes non-obstructive azoospermia in infertile men. J Med Genet. 2017;54:633-9.

[11] Wang WH, Feng YM, Dong J, Zhou Z, Jing J, Li ZX, et al. A Novel Compound Heterozygous Mutation in TDRD9 Causes Oligozoospermia. Reprod Sci. 2024;31:3413-9.

[12] Hu K, Sha X, Zu C, Yang F, Wang G, Cheng H, et al. Novel homozygous variants in piRNA pathway factors lead to male infertility in humans. Reproductive BioMedicine Online. 2025;51:104974.

[13] Babakhanzadeh E, Khodadadian A, Rostami S, Alipourfard I, Aghaei M, Nazari M, et al. Testicular expression of TDRD1, TDRD5, TDRD9 and TDRD12 in azoospermia. Bmc Med Genet. 2020;21.

[14] Chénais B, Caruso A, Hiard S, Casse N. The impact of transposable elements on eukaryotic genomes: From genome size increase to genetic adaptation to stressful environments. Gene. 2012;509:7-15.

[15] Richardson Sandra R, Doucet Aurélien J, Kopera Huira C, Moldovan John B, Garcia-Perez José L, Moran John V. The Influence of LINE-1 and SINE Retrotransposons on Mammalian Genomes. Microbiology Spectrum. 2015;3:10.1128/microbiolspec.mdna3-0061-2014.

[16] Penzkofer T, Jäger M, Figlerowicz M, Badge R, Mundlos S, Robinson PN, et al. L1Base 2: more retrotransposition-active LINE-1s, more mammalian genomes. Nucleic Acids Research. 2017;45:D68-D73.

[17] Tao J, Wang Q, Mendez-Dorantes C, Burns KH, Chiarle R. Frequency and mechanisms of LINE-1 retrotransposon insertions at CRISPR/Cas9 sites. Nature Communications. 2022;13:3685.

603 [18] Zhou H, Yin Z, Ni B, Lin J, Luo S, Xie W. Whole exome sequencing analysis of 167 men with primary
604 infertility. BMC Medical Genomics. 2024;17.
605 [19] Bao Z, Wang Y, Wang R, Dong F, Li T, Chan W-Y, et al. Pathogenic TDRD12 variants cause defective
606 piRNA pathway and male infertility in humans and mice. Journal of Genetics and Genomics.
607 2024;51:1322-6.
608 [20] Brouha B, Schustak J, Badge RM, Lutz-Prigge S, Farley AH, Moran JV, et al. Hot L1s account for the
609 bulk of retrotransposition in the human population. Proceedings of the National Academy of Sciences.
610 2003;100:5280-5.
611 [21] Beck CR, Collier P, Macfarlane C, Malig M, Kidd JM, Eichler EE, et al. LINE-1 Retrotransposition
612 Activity in Human Genomes. Cell. 2010;141:1159-70.
613

## Supplementary Files

This is a list of supplementary files associated with this preprint. Click to download.

- sup2.docx
- SupplementaryTable2.xls